Molecular Adsorption on ZnO(10$\bar{1}$0) Single-Crystal Surfaces: Morphology and Charge Transfer

ARTICLE *in* LANGMUIR · JUNE 2012

Impact Factor: 4.46 · DOI: 10.1021/la301347t · Source: PubMed

5 AUTHORS, INCLUDING:

Jixin Chen
Ohio University
45 PUBLICATIONS **1,195** CITATIONS
SEE PROFILE

Lee Bishop
University of Wisconsin–Madison
17 PUBLICATIONS **293** CITATIONS
SEE PROFILE

Robert J. Hamers
University of Wisconsin–Madison
384 PUBLICATIONS **17,284** CITATIONS
SEE PROFILE

Langmuir

Article

pubs.acs.org/Langmuir

Molecular Adsorption on ZnO(10$\bar{1}$0) Single-Crystal Surfaces: Morphology and Charge Transfer

Jixin Chen, Rose E. Ruther, Yizheng Tan, Lee M. Bishop, and Robert J. Hamers*

Department of Chemistry, University of Wisconsin—Madison, 1101 University Avenue, Madison, Wisconsin 53706, United States

Supporting Information

ABSTRACT: While ZnO has excellent electrical properties, it has not been widely used for dye-sensitized solar cells, in part because ZnO is chemically less stable than widely used TiO_2. The functional groups typically used for surface passivation and for attaching dye molecules either bind weakly or etch the ZnO surface. We have compared the formation of molecular layers from alkane molecules with terminal carboxylic acid, alcohol, amine, phosphonic acid, or thiol functional groups on single-crystal zinc oxide (10$\bar{1}$0) surfaces. Atomic force microscopy (AFM) images show that alkyl carboxylic acids etch the surface whereas alkyl amine and alkyl alcohols bind only weakly on the ZnO(10$\bar{1}$0) surface. Phosphonic acid-terminated molecules were found to bind to the surface in a heterogeneous manner, forming clusters of molecules. Alkanethiols were found to bind to the surface, forming highly uniform monolayers with some etching detected after long immersion times in an alkanethiol solution. Monolayers of hexadecylphosphonic acid and octadecanethiol were further analyzed by Fourier transform infrared spectroscopy (FTIR), X-ray photoelectron spectroscopy (XPS), and electrochemical measurements. AFM scratching shows that thiols were bound strongly to the ZnO surface, suggesting the formation of strong Zn−S covalent bonds. Surprisingly, the tridentate phosphonic acids adhered much more weakly than the monodentate thiol. The influence of organic grafting on the charge transfer to ZnO was studied by time-resolved surface photovoltage measurements and electrochemical impedance measurements. Our results show that the grafting of thiols to ZnO leads to robust surfaces and reduces the surface band bending due to midgap surface states.

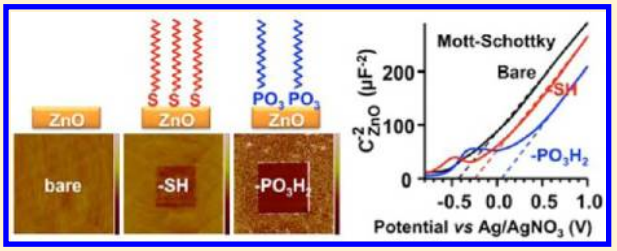

INTRODUCTION

We report here a comparison of the interaction of undecanol, octadecanoic acid, dodecylamine, hexadecylphosphonic acid, and octadecanethiol with single-crystal ZnO(10$\bar{1}$0) surfaces. ZnO has many favorable properties including good transparency, high electron mobility, a wide band gap, piezoelectricity, strong room-temperature luminescence, and, most importantly, low cost, which have led to its widespread application in transistors, light-emitting diodes, sensors, and solar cells.[1−4] In principle, ZnO should also be a better anode material for dye-sensitized solar cells (DSSCs) than the more commonly used TiO_2 because it has a much higher carrier mobility.[5,6] However, the best-performing ZnO dye-sensitized solar cells achieve only about half of the efficiency of their TiO_2 analogues.[7]

For ZnO-based biosensors such as the quartz crystal microbalance (QCM) and thin-film bulk acoustic wave resonator (TBAR), little work has been performed on the direct surface functionalization of ZnO except for some initial studies using carboxylic acids, organosilanes, or relatively weak electrostatic interactions.[8−11] In many reports on ZnO-based solar cells, the functional groups used to bind to ZnO electrodes were the same as those used successfully on TiO_2 electrodes. For example, carboxylic acids are commonly used as linkers for dyes, and *tert*-butyl alcohol and/or 4-tertbutylpyridine are typical coadsorbing molecules for surface passivation.[2,7,12] However, poor dye loading and poor chemical passivation have limited the efficiency of ZnO-based DSSCs.[2,12,13] The former limits the ability to absorb sunlight, and the latter limits the open circuit potential and fill factor. Using time-resolved photoconductivity measurements, Tiwana and co-workers recently reported that the relatively slow electron injection from dye molecules into ZnO compared to that into TiO_2 could be attributed to the carboxylic acid group that is commonly used to link the dyes to the surface.[14,15] Thus, finding proper binding groups and passivations for ZnO is essential to improving the performance of these devices.[16−22]

Here, we report an investigation of the interaction of different functional groups with ZnO surfaces. We have chosen to work with undecanol, octadecanoic acid, dodecylamine, hexadecylphosphonic acid, and octadecanethiol as model systems. All of these molecules consist of a long alkyl chain (12−18 carbons) with a single terminal functional group. Long-chain alkanes are excellent model molecules because they will stabilize the monolayers on the surface and are ideal for morphology studies. Phosphonic acids and thiols are often regarded as the most promising types of molecules that form strong covalent bonds on ZnO surfaces, and thus they have been widely studied.[23−27] However, many of these studies were done on nanocrystalline

Received: April 2, 2012
Revised: June 6, 2012
Published: June 8, 2012

surfaces where the morphologies of the monolayers on the ZnO surface were not characterized. Recently, we used atomic force microscopy (AFM) to study the formation of organic layers produced on single-crystal ZnO by photochemical grafting.[28] Here, we use the same approach to study monolayers produced by thermal grafting. Our results show that undecanol, octadecanoic acid, and dodecylamine do not form stable self-assembled monolayers (SAMs) on ZnO($10\bar{1}0$) surfaces whereas hexadecylphosphonic acid and octadecanethiol both form stable monolayers. However, there are pronounced differences in the resulting morphologies. To investigate the influence of surface molecules on the surface states of ZnO, time-resolved surface photovoltage (SPV) measurements were performed. Finally, charge transfer across the ZnO−electrolyte interfaces was studied via Mott−Schottky plots.

EXPERIMENTAL SECTION

Single-crystal zinc oxide ZnO($10\bar{1}0$) (CrysTec GmbH, Germany) substrates were annealed in a ZnO kiln (constructed from ZnO sputter targets, Kurt J. Lesker, 99.999%) at 1050 °C for 3 h. This procedure has been shown to produce very flat surfaces with well-defined terraces and steps.[29] The ZnO($10\bar{1}0$) surface was studied because it is the most stable and abundant surface on many ZnO nanostructures.[2] After being annealed, the substrates were functionalized with different ligands. In a typical functionalization procedure, the substrates were soaked in a 1 mM solution of the ligand in ethanol at room temperature or 50 °C overnight. This procedure was used for octadecanoic acid (ODA, 95%, Sigma-Aldrich), hexadecylphosphonic acid (HDPA, 97%, Sigma-Aldrich), octadecanethiol (ODT, 98%, Sigma-Aldrich), and dodecylamine (99%, Sigma-Aldrich). For the undecanol functionalization, the substrates were soaked in the neat liquid (99%, Sigma-Aldrich) at 80 °C for 3 h.

The molecular layers on ZnO were then imaged using an atomic force microscope (AFM, Veeco Nanoscope IVa). Tapping-mode diamond-like-carbon-coated tips (Tap300Al-G-DLC, Budget Sensors, Bulgaria) were used for imaging and also monolayer removal via scratching. The scratching was carried out in contact mode at a fixed scan rate of 20 μm/s and different loading forces. The loading force was proportional to the approaching set point voltage, which was adjusted to 0 V before tip−sample approach. The actual force applied to the surface can be estimated by measuring the force−distance curves. Using the average spring constant of the tips, the loading force was roughly estimated to be ∼2 μN/V. Molecules were typically scratched away from a region 2×2 μm^2, with 512 scan lines. After the removal of the molecular layer using the AFM tip, a lower force at ∼0.05 V (force ≈ 100 nN) or tapping mode was used to image a larger area. In some cases, the contact-mode scan at 0.05 V was also used to clean the debris near the scratched surface. When debris adhered to the tip and affected the imaging quality, a fast tapping-mode scan, ∼200 μm/s over a 50×50 μm^2 area, was used to clean the tip.

XPS data were obtained using a custom-built XPS system (Physical Electronics Inc., Eden Prairie, MN) consisting of a model 10-610 Al Kα source (1486.6 eV photon energy) with a model 10-420 toroidal monochromator and a model 10-360 hemispherical analyzer with a 16-channel detector array; measurements were typically performed using an electron takeoff angle of 45° and an analyzer pass energy of 23.5 eV (yielding an analyzer resolution of 0.35 eV). The error in the measurement of XPS peak intensity was estimated to be ∼10%. The atomic sensitivity factors (ASF) were obtained from the literature for C 1s (0.296), Zn $2p_{3/2}$ (3.354), O 1s (0.711), P 2s (0.38), S 2p (0.57), and Au 4f (5.24).[30] To compensate for any sample charging, the main C 1s peak was shifted to 284.8 eV and all other peaks were shifted by the same amount. The peaks after linear and Shirley background removal were fit with Voigt functions that were ∼90% Gaussian and ∼10% Lorentzian using Fityk software.[31] For P 2s and S 2p peaks, the backgrounds were fit using cubic polynomial functions because the Zn 3s shakeup peak introduces a curved background in the region of these peaks.[30]

Fourier transform infrared spectroscopy (FTIR) data were obtained with a Bruker Vertex 70 equipped with a Veemax II variable-angle single-bounce reflection accessory using a liquid-nitrogen-cooled HgCdTe detector. Measurements shown in this article were collected using s-polarized light at an angle of incidence of 30° from the surface normal.

Time-resolved surface photovoltage (SPV) measurements were carried out using nanocrystalline ZnO films (100 nm particle size, Sigma-Aldrich) made in a manner similar to that of nanocrystalline TiO_2 films.[32] Nanocrystalline films were used because the strong piezoelectric effect of single-crystal ZnO induced strong oscillations in SPV measurements. For SPV measurements, the ZnO nanocrystalline films served as the working electrode and were deposited on FTO glass. The films were separated from the sensing electrode (a second piece of clean FTO-coated glass) by a 25-μm-thick Surlyn 1720 polymer spacer. The capacitance C_{air} is ∼35 pF for our ∼1 cm^2 electrodes separated ∼25 μm by air. The spacer had a hole in the center that allowed brief pulses of tunable laser light (5 ns pulse width, 20 Hz pulse rate, 4 mm diameter) from an Ekspla NT342B tunable Nd:YAG laser source to illuminate the sample. Although experiments were conducted at various wavelengths, data shown here used a wavelength of 370 nm and a fluence of ∼0.043 ± 0.002 mJ/pulse. The laser fluence was measured using a Coherent Field MaxII photodetector. The resulting surface photovoltage was measured using an Agilent DSO5054A 500 MHz oscilloscope (50 Ω, dc coupling) directly connected to the sample and sensing electrode. The voltage data were then integrated with time and divided by 50 Ω to represent the change in the surface photocharge on the FTO sensing electrode.

Electrochemical measurements were carried out with a Metrohm Autolab analyzer using a standard three-electrode setup and a custom-built Teflon cell. Single-crystal ZnO($10\bar{1}0$) samples were sealed against the cell using a Kalrez O-ring (Dupont), exposing the central region (area ∼0.38 cm^2) to an electrolyte solution. A platinum wire served as the counter electrode. A single-junction Ag/Ag^+ reference electrode was made by immersing a Ag wire in 0.01 M $AgNO_3$ and 0.1 M tetrabutylammonium hexafluorophosphate (TBAPF, Sigma-Aldrich) in acetonitrile. The reference electrode was confirmed to be stable before and after the measurements at ∼+0.34 V versus a standard Ag/AgCl/saturated NaCl reference electrode that corresponds to ∼0.54 V versus SHE, consistent with previous reports.[33] TBAPF (0.1 M) in acetonitrile was used as the electrolyte for all studies. Fresh electrolyte solutions for the sample compartment and the reference electrode were used for each measurement. The sample potential was scanned from −0.8 V to +1 V versus the reference electrode, and 10 mV ac modulation at 10, 100, 1K, 10K, and 100K Hz frequencies was applied to the impedance measurements. The data was fit by an $R(RC)$ equivalent-circuit model, and the inverse square of the surface capacitance was plotted versus the applied dc bias to generate the Mott−Schottky plots.[3435]

RESULTS

Atomic Force Microscopy (AFM) Measurements. A simple way to characterize organic monolayers on a substrate is to dislodge the layers mechanically using an AFM tip with an appropriate loading force.[28,36] First, the force necessary to damage the substrate was determined by scratching a clean substrate in contact mode and then imaging the surface either in contact mode using a lower loading force or in tapping mode. Once the damage threshold was determined, organic monolayers were removed using more moderate loading forces. Detailed procedures for this testing are provided in the Supporting Information.

Figure 1 shows AFM images of the surfaces after immersion in solutions of each of four different ligands. The surface that was exposed to $C_{17}H_{35}COOH$ (Figure 1b) is clearly etched with many pits as deep as several nanometers. However, the surfaces exposed to $CH_3(CH_2)_{17}SH$ (Figure 1a), $C_{11}H_{23}OH$ (Figure 1c), and $C_{12}H_{25}NH_2$ (Figure 1d) show flat terraces and steps, with no evidence of etching. We note that there is some variation in step density on different samples due to different degrees of sample

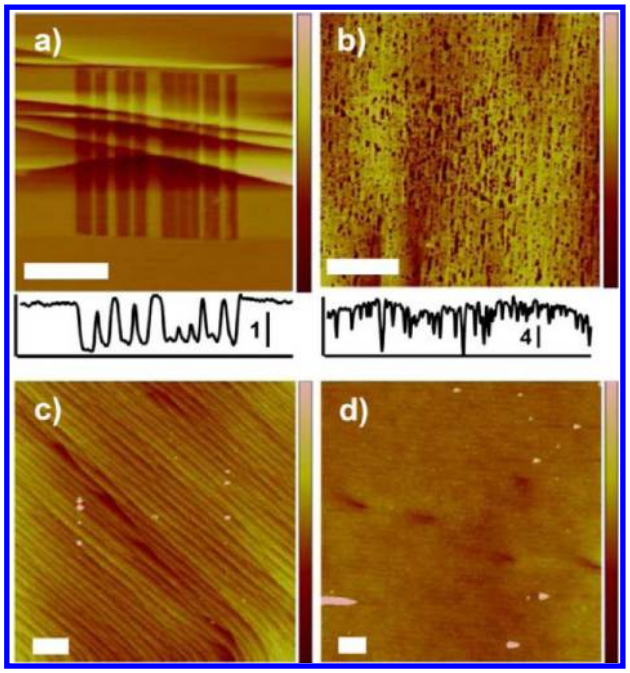

Figure 1. Tapping-mode AFM topographical images of ZnO(10$\bar{1}$0) after grafting in a 1 mM ethanol solution of (a) $C_{18}H_{37}SH$ (bands scratched by the AFM tip), (b) $C_{17}H_{35}COOH$, (c) $C_{11}H_{23}OH$ (neat), and (d) $C_{12}H_{25}NH_2$. The center 2 × 2 μm^2 in b–d is scratched by AFM at 1 V, and the center 5 × 5 μm^2 in c and d are scanned by contact AFM at 0.02 V. All *x* scale bars are 1 μm, and all *z* scale bars are 10 nm. Note that different step-edge structures of the four samples come from the annealing of different crystals with slightly different degrees of sample miscut.

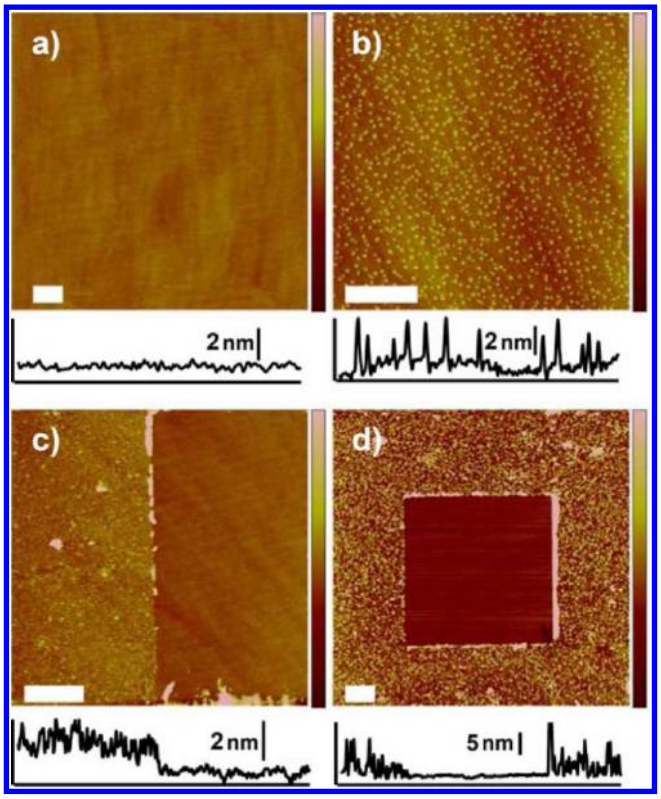

Figure 2. AFM topographical images of ZnO (10$\bar{1}$0) (a) before grafting in 1 mM hexadecylphosphonic acid solution in ethanol and grafted for (b) 5 min at room temperature, (c) overnight at room temperature, and (d) overnight at 50 °C. The right portion of panel c and the central region of panel d were scratched by the AFM tip. The *x* scale bars are 1 μm, and the *z* scale bars are 10 nm.

miscut. In repeated experiments, we have shown that these different step densities do not impact the overall monolayer formation reported here. For each of these four molecules, we evaluated whether any monolayers were detected by AFM using the scratching procedure described above. In repeated attempts, we failed to detect any evidence of molecular-layer formation with the carboxylic acid, alcohol, and amine functional groups. However, the thiol group forms a well-defined layer; Figure 1a shows patterns that were created using an increased loading force. The ability to make and image stable patterns in this manner demonstrates that the octadecanethiol molecule forms well-defined, homogeneous monolayers on ZnO(10$\bar{1}$0).

Figure 2 shows the ZnO(10$\bar{1}$0) surface before (Figure 2a) and after (Figure 2b–d) exposure to $C_{16}H_{33}PO_3H_2$; Figures 2c and 3d include both grafted regions and regions where the molecular layers were subsequently removed using the AFM tip. Although the starting surface (Figure 2a) appears very smooth, after immersion in $C_{16}H_{33}PO_3H_2$ for only 5 min the AFM image in Figure 3b (Figure 2b) shows that the surface is covered with islands of nanoclusters with a height of ∼2 nm and an apparent diameter of ∼30 nm (possibly broadened by the AFM tip) separated by ∼100 nm (Figure 2b). Immersion for longer times of ∼16 h (Figure 2c) leads to the further growth of larger islands on the surface with the same height (Figure 3c). The height of the nanocluster can also grow if a longer time or elevated temperatures are employed, as demonstrated by the growth at 50 °C shown in Figure 2d. Overall, the adsorbed molecules do not form homogeneous monolayers, and no evidence of etching is observed.

Figure 3 shows AFM images before and after a ZnO(10$\bar{1}$0) surface was exposed to the octadecanethiol solution for 5 min. The AFM image (Figure 3b) shows a very uniform layer. Contact-mode AFM images show that the monolayer is ∼1.3 nm higher than the underlying substrate. Over extended periods of time during scanning for ∼20 min, the scratch disappears; we attribute this to the diffusion of molecules from the AFM tip and from regions surrounding the scratched area. No noticeable etching on the ZnO surface is observed. However, when the ZnO sample is exposed to the octadecanethiol solution at 50 °C for 16 h the surface roughens considerably with the formation of many holes ∼2 nm in depth (Figure 3c). When the octadecanethiol layer is scratched away by an AFM tip, the underlying ZnO surfaces also show pits (Figure 3d). The formation of pits in the ZnO surface shows that octadecanethiol induces some small amount of etching of the surface at long times.

Surprisingly, significantly different forces are required to dislodge the $C_{16}H_{33}PO_3H_2$ and $C_{18}H_{37}SH$ monolayers mechanically, even when using the same AFM tip for both experiments. In Figure 2, a small scratching force and an ∼0.02 V cantilever deflection (force ∼40 nN) in contact mode is able to remove the $C_{16}H_{33}PO_3H_2$ molecules. However, on a $C_{18}H_{37}SH$ grafted surface (Figure 3), a minimum loading of 0.5 V (∼1 μN) is required to scratch the grafted $C_{18}H_{37}SH$ monolayer. Further details are provided in the Supporting Information.

The above experiments show that $C_{17}H_{35}COOH$, $C_{12}H_{25}NH_2$, and $C_{11}H_{23}OH$ do not form stable monolayers on ZnO(10$\bar{1}$0) whereas both $C_{18}H_{37}SH$ and $C_{16}H_{33}PO_3H_2$ do. These differences can also be observed by visual inspection: immediately after removal from the solution, all surfaces are hydrophobic, but after

dx.doi.org/10.1021/la301347t | *Langmuir* 2012, 28, 10437–10445

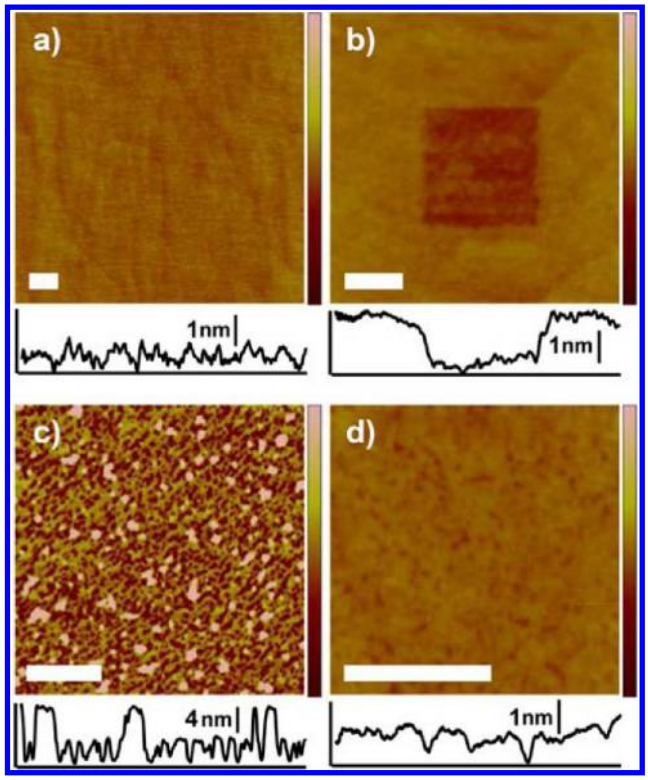

Figure 3. AFM topographical image of ZnO(10$\bar{1}$0) (a) before grafting in 1 mM octadecanethiol solution in ethanol, (b) grafted overnight at room temperature and imaged in contact mode at 0.05 V after the center of the image was scratched at 0.5 V, and (c) grafted for 16 h at 50 °C and imaged in tapping mode. (d) High-resolution image of the scratched area from sample c, showing the formation of pits in the underlying ZnO. The vertical height range is 10 nm for all images; *x* scale bars are 1 μm in a and b and 500 nm in c and d. For each image, a height profile with a vertical scale bar (on the order of nanometers) is also included.

being rinsed with acetone and methanol, only $C_{18}H_{37}SH$ and $C_{16}H_{33}PO_3H_2$ remain hydrophobic.

Fourier Transform Infrared Spectroscopy Measurements (FTIR). FTIR measurements were performed to characterize the molecular layers produced by octadecanethiol and by hexadecylphosphonic acid. FTIR shows that both molecules have their asymmetric CH_2 stretching peak at ~2918 cm^{-1} and their symmetric stretching peak at ~2850 cm^{-1} (Figure 4). These values are the same as those observed for the

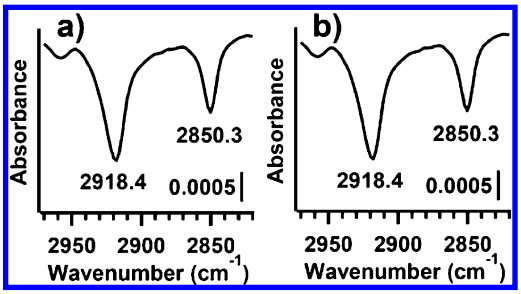

Figure 4. FTIR of single-crystal ZnO(10$\bar{1}$0) samples that have been grafted in (a) $C_{16}H_{33}PO_3H_2$ and (b) $C_{18}H_{37}SH$, respectively.

nearly crystalline thiol SAMs on gold, indicating that the alkane tails are close-packed, forming a dense, nearly crystalline phase.[37] We do not observe variations in these FTIR peak values for the samples that are grafted for longer times.

X-ray Photoelectron Spectroscopy Measurements (XPS). The intensities, the binding energies, and the shape of the high-resolution XPS peaks contain useful clues for the chemical environments of the elements. Quantitative analysis of the XPS spectra indicates that the monolayers of hexadecylphosphonic acid and octadecanethiol have molecular densities of ~4.4 and ~4.2 molecules/nm^2 respectively (Figure 5 and Table 1). Detailed calculations are described in the Supporting Information. For comparison, we also prepared a conventional self-assembled monolayer on gold using a 100-nm-thick gold film on silicon that was soaked in a 1 mM solution of $C_{18}H_{37}SH$ in ethanol overnight. By XPS, the thiol on gold had a density of 3.9 molecules/nm^2. These coverage values of thiol on ZnO, phosphonic acid on ZnO, and thiol on gold are close to the value of ~4.6 molecules/nm^2 reported previously for high-quality, close-packed alkyl monolayers on gold.[38] This provides further evidence that high-quality monolayers of thiols and hexadecylphosphonic acid are formed on ZnO, consistent with our AFM and FTIR observations.

In addition to the areas of the high-resolution XPS peaks, the binding energies and shapes of the peaks are also useful clues to the chemical environment of the elements. The main information in the C 1s peak is the area, which is used to calculate the surface coverage of the organic molecules. For Zn $2p_{3/2}$ peaks, an obvious change is that the intensity decreases after grafting (Figure 5 and Table 1). This is because the organic layers inelastically scatters some of the photoelectrons from Zn. (See the Supporting Information for a numerical estimate of this effect.) Although the binding energy of the Zn $2p_{3/2}$ peak at ~1023 eV does not change significantly after grafting, there are clear differences in the full-width at half-maximum (fwhm). The fwhm of the Zn $2p_{3/2}$ peak is 1.12 ± 0.06 eV for the clean surface, 1.16 ± 0.01 eV for $C_{16}H_{33}PO_3H_2$ grafted samples, and 0.94 ± 0.01 eV for $C_{18}H_{37}SH$ grafted samples. The phosphonic acids do not change the fwhm of the Zn $2p_{3/2}$ peak, but exposure to the thiols actually *reduces* it by ~16%. Both the $C_{16}H_{33}PO_3H_2$ and $C_{18}H_{37}SH$ grafted samples have C 1s peaks with a fwhm of 0.66 ± 0.02 eV. Because these values are the same, we conclude that the differences in the width of the Zn $2p_{3/2}$ are real and not a result of possible artifacts such as sample charging.

All of the O 1s peaks can be fit by two Voigt peaks at ~531.5 and ~530.5 eV; the relative intensities of these two components change with grafting. We observe that the ratio between the 531.5 eV peak and 530.5 peak increases after hexadecylphosphonic acid grafting but decreases after octadecanethiol grafting (Figure 5). The increase in the relative intensity of the 531.5 eV peak after the grafting of hexadecylphosphonic acid is consistent with previous work showing that this peak arises from hydroxyl groups and grafted phosphonic acid molecules whereas the peak at 530.5 eV is attributed to O atoms in the underlying bulk ZnO.[27] The decrease in relative intensity of the 531.5 eV peak indicates that sulfur in the thiol group *replaces* the ZnO surface oxygen.[25] The S 2p peak can be fit by two Voigt functions with a 2:1 area ratio and a separation of ~1.3 eV, as expected from the spin−orbit splitting into S $2p_{3/2}$ and S $2p_{1/2}$ components. The binding energy of the S $2p_{3/2}$ peak, 162 eV, is the same as that observed on gold (Table 2). No other peaks are observed in the S 2p region. This indicates that the thiol-modified surfaces are free of oxidized sulfur species, which have peaks around 166−170 eV.[25,39] In addition, the nonspecific binding of thiols has been reported to give S $2p_{3/2}$ near 163.6 eV.[40]

The quantitative analysis of XPS data is often limited by uncertainty in the electron escape depths. Because the measured

dx.doi.org/10.1021/la301347t | *Langmuir* 2012, 28, 10437−10445

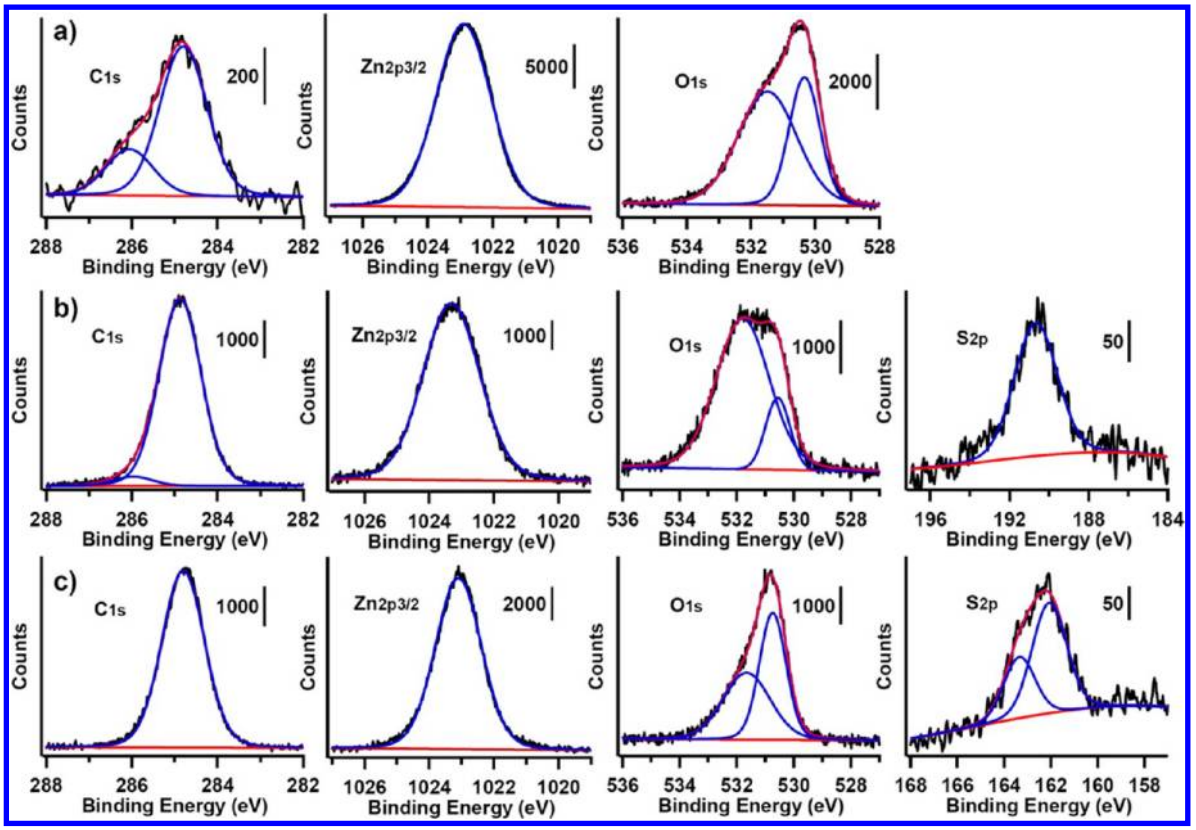

Figure 5. XPS spectra of (a) a clean ZnO($10\bar{1}0$) sample and samples that have been grafted in (b) $C_{16}H_{33}PO_3H_2$ (the same sample as in Figure 2c) and (c) $C_{18}H_{37}SH$ (the same sample as in Figure 3b). These three ZnO samples (0.5×0.5 cm^2) are fractions of the same piece of a larger ZnO($10\bar{1}0$) single crystal (1×1 cm^2).

Table 1. XPS Peak Intensities of ZnO($10\bar{1}0$) Samples (ASF-Corrected)

sample		C 1s		$Zn2p_{3/2}$	O 1s		P 2s	coverage (nm^{-2})[a]
clean ZnO	BE (eV)	286.1	284.8	1022.9	531.5	530.3		
	intensity	795	2.56×10^3	1.37×10^4	1.39×10^4	8.26×10^3		
ZnO_$C_{16}H_{33}PO_3H_2$	BE (eV)	286.0	284.8	1023.2	531.7	530.5	190.6	
	intensity	997	2.10×10^4	4.26×10^3	9.81×10^3	2.00×10^3	1.20×10^3	4.4

sample		C 1s	Zn $2p_{3/2}$	O 1s		S $2p_{1/2}$	S $2p_{3/2}$	coverage (nm^{-2})[a]
ZnO_$C_{18}H_{37}SH$	BE (eV)	284.8	1023.1	531.7	530.7	163.3	162.1	
	intensity	2.00×10^4	5.66×10^3	5.35×10^3	5.74×10^3	282	564	4.2

sample		C 1s	Au $4f_{5/2}$	Au $4f_{7/2}$	S $2p_{1/2}$	S $2p_{3/2}$	coverage (nm^{-2})[a]
Au_$C_{18}H_{37}SH$	BE (eV)	284.8	87.0	83.3	163.2	161.7	
	intensity	1.90×10^4	5.02×10^3	5.86×10^3	380	759	3.9

[a]Values are reported in molecules/nm^2. See the Supporting Information for detailed calculations.

Table 2. XPS Peak Area Ratios

sample	A_O/A_{Zn}[a]	A_C/A_{Zn}	A_C/A_P	A_C/A_S
ZnO_clean	1.62	0.3		
ZnO_$C_{16}H_{33}PO_3H_2$_overnight	2.77	5.16	18.70	
then 50 °C overnight	3.42	6.64	18.45	
ZnO_$C_{18}H_{37}SH$_overnight	1.96	3.53		23.56
then 50 °C overnight	2.18	4.01		16.59

[a]A_X is the sensitivity-factor-corrected peak area of element X.

intensities and the atomic sensitivity factors are often known to good precision, the sensitivity-factor-corrected intensity ratios can serve as a sensitive indicator of changes in the surface chemistry. For example, the corrected area ratio A_O/A_{Zn} in clean ZnO($10\bar{1}0$) is ~1.6:1 (Table 2). This value is consistent with the 1:1 Zn/O stoichiometry ratio of the nonpolar ZnO($10\bar{1}0$) surface given the fact that the electron mean free path for O 1s electrons is 1.8 nm versus 1.07 nm for the Zn 3d electrons (eq S2 and Table S2 in the SI).[41,42] The A_C/A_{Zn} ratio on hexadecylphosphonic acid grafted samples is ~5.2. This value agrees well with the estimated A_C/A_{Zn} ratio for a 2.0 nm organic monolayer, which is ~6.4 (eq S5 and Table S2 in the SI). The octadecanethiol grafted sample has $A_C/A_{Zn} \approx 3.5$, which increases to 4.01 with increasing grafting time and higher packing density. The ratios A_C/A_P (for the phosphonic acid) and A_C/A_S (for octadecanethiol) are expected to be ~30 if the 2 nm carbon layer is on top of the functional groups. However, A_C/A_P and A_C/A_S ratios that are less than or close to 20 are observed.

dx.doi.org/10.1021/la301347t | *Langmuir* 2012, 28, 10437−10445

Angle-resolved XPS was performed to investigate the peak area ratios for the surface molecules further.

Angle-resolved XPS has been used to identify the relative depth of the elements from the surface because the surface elements contribute more to the total XPS signal at larger electron takeoff angles.[43] Figure 6 shows that for $C_{16}H_{33}PO_3H_2$

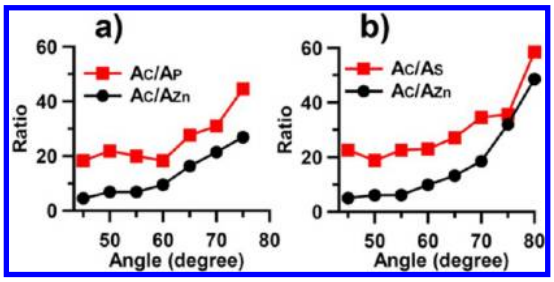

Figure 6. Angle-resolved XPS measurements of samples that have been grafted in (a) $C_{16}H_{33}PO_3H_2$ (the same sample as in Figure 2c) and (b) $C_{18}H_{37}SH$ (the same sample as in Figure 3b). Angles are measured from the surface normal.

grafted to ZnO($10\bar{1}0$) the A_C/A_{Zn} and A_C/A_P ratios increase as electrons are measured at larger angles, farther from the surface normal. The increase in A_C/A_P indicates that the hexadecylphosphonic acid molecules are aligned with the hydrophobic alkane tails stretching away from the ZnO surface whereas the phosphonic acid head groups are at the molecule−ZnO interface. Similar geometry is observed for octadecanethiol (Figure 6b). These results are consistent with prior XPS measurements using shorter hexylphosphonic acids.[23]

Surface Photovoltage Measurements (SPV). In our apparatus, the surface photovoltaic response is measured by capacitively coupling to a "sense" electrode and passing the resulting displacement current I_{dis} across the 50 Ω input impedance of a fast amplifier with gain G. The amplifer produces a voltage equal to $V_{out} = GI_{dis}R_{inp} = GRC\ d(SPV)/dt$ that must average to zero over long time intervals because of the capacitive coupling. In Figure 7,

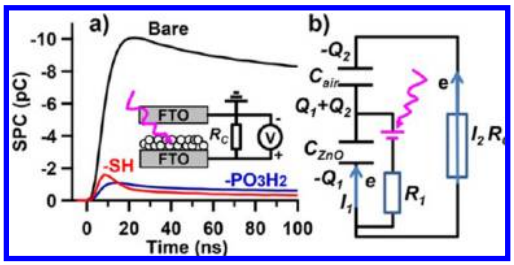

Figure 7. (a) Time-resolved measurement of interfacial charge separation at bare, $C_{16}H_{33}PO_3H_2$-modified ($-PO_3H_2$), and $C_{18}H_{37}SH$ modified (−SH) films presented as the charge transferred vs time. The inset shows the circuit with a coupling resistance of R_C = 50 Ω. (b) Equivalent circuit where R_1 is the resistance for charge transfer across the space-charge layer, C_{ZnO} and C_{air} are the space-charge capacitances of ZnO and the capacitance of the electrodes, respectively, I_1 and I_2 are electron currents, and Q_1 and Q_2 are charges.

we present the integrated signal $\int_o^t V_{out}/GR = \int_o^t I_{dis}(t) = Q(t)$, which represents the charge transferred. The curve shows a fast increase immediately after and then an ∼3 ns laser pulse due to the initial charge separation in the space-charge layer, followed by a slower return to zero as surface recombination restores the system to equilibrium; this region can be fit with an exponential decay function: $-Q_{SPV} = Ae^{-t/\tau}$, where τ is the decay time constant (Figure 7a). In our experiment, the negative current shows that excess electrons produced near the surface move toward the bulk while the excess holes remain at or near the surface.

Figure 7 shows plots of the time-resolved charge transfer for ZnO samples with different surface functional groups. These data show that surface functionalization has several effects. First, there is less charge separation when the surfaces are modified compared to the bare sample. For example, on the bare sample each laser pulses yields a charge separation corresponding to $Q_{SPV} = 1.0 \times 10^{-11}$ C, whereas $-Q_{SPV} = 1.1 \times 10^{-12}$ C for the $C_{16}H_{33}PO_3H_2$-modified surface and 1.6×10^{-12} C for the $C_{18}H_{37}SH$-modified surface. Second, faster decay rates were observed when the surfaces were modified. The average decay times τ of surface photocharges follow the order ZnO-bare (4.9 μs) > ZnO-$C_{16}H_{33}PO_3H_2$ (2.2 μs) > ZnO-$C_{18}H_{37}SH$ (0.44 μs).

Mott−Schottky Data. The band bending can be further studied electrochemically. The overall electrochemical response of the surface is controlled by a number of different processes and is usually described by an equivalent circuit that consists of the cell resistance in series with the resistance to charge transfer and the space-charge capacitance;[44] this model is identical to that discussed earlier for the time-resolved SPV measurements. At low frequencies, one of the important parameters is the space-charge capacitance; when in depletion, the capacitance varies with potential according to the Mott−Schottky equation for an n-type semiconductor[35,45]

$$\frac{1}{C_{ZnO}^2} = \frac{2}{\varepsilon\varepsilon_0 e N_D A^2}\left(\phi_{ZnO} - \frac{kT}{e}\right) \quad (1)$$

where C_{ZnO} is the capacitance of the ZnO space-charge region, ε is the permittivity of the ZnO space-charge region, ε_0 is the permittivity of free space, e is the carrier electron charge, N_D is the carrier density of ZnO, A is the measured surface area, k is the Boltzmann constant, and T is the temperature. $\phi_{ZnO} = \Psi_{ZnO} - \Psi_{FB}$ is the band bending of ZnO near the ZnO−electrolyte interface, where Ψ_{ZnO} is the potential of the ZnO electrode and Ψ_{FB} is the flat-band potential at which $\phi_{ZnO} = 0$.

A plot of $1/C^2_{ZnO}$ versus potential Ψ_{ZnO} generates the well-known Mott−Schottky plot (Figure 8). At intermediate

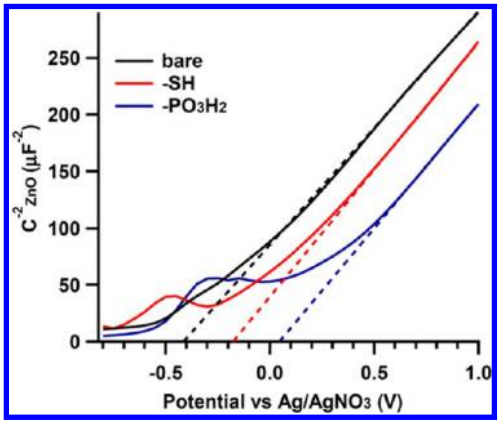

Figure 8. Mott−Schottky plots (1 kHz) of bare and $C_{16}H_{33}PO_3H_2$ ($-PO_3H_2$)- and $C_{18}H_{37}SH$ (−SH)-modified ZnO($10\bar{1}0$) single-crystal samples. The dashed lines indicate the linear parts of the curves.

potentials, each curve has a nonlinear part extending from ∼−0.6 to ∼0.2 V for bare ZnO, from −0.6 to ∼0.4 V for $C_{18}H_{37}SH$-modified ZnO, and from −0.6 to ∼0.5 V for $C_{16}H_{33}PO_3H_2$-modified ZnO. At 0 potential versus the Ag/$AgNO_3$ reference, $1/C_{ZnO}^2$ equals 88 μF^{-2} for ZnO-bare, 62 μF^{-2}

dx.doi.org/10.1021/la301347t | Langmuir 2012, 28, 10437−10445

for ZnO-$C_{18}H_{37}SH$, and 53 μF^{-2} for ZnO-$C_{16}H_{33}PO_3H_2$. At more positive potential, the curves increase linearly. The nonlinear Mott−Schottky behavior in the range between ∼−0.6 and +0.4 V arises from the presence of surface states, which are not accounted for in the usual Mott−Schottky model or in eq 1.[35]

According to eq 1, the flat-band potentials were derived from the intercept of the linear parts of the Mott−Schottky plots with the voltage axis. After the thermal voltage term was corrected for, the resulting flat-band potentials versus $Ag/AgNO_3$ are −0.42 ± 0.01 V for ZnO-bare, −0.21 ± 0.01 V for ZnO-$C_{18}H_{37}SH$, and 0.00 ± 0.01 V for ZnO-$C_{16}H_{33}PO_3H_2$. (The standard deviations of the fittings are used to calculate the errors.) The carrier densities are also calculated from the Mott−Schottky plots. The slopes of the linear curves are parallel to each other at $(2.1 \pm 0.1) \times 10^{14}$ F^{-2} V^{-1}, which is consistent with the fact that the slopes are defined by the same carrier concentration of the same ZnO sample with different surface modifications. With this slope value, using an area $A = (3.8 \pm 0.3) \times 10^{-5}$ m^2, permittivity $\varepsilon = 8.5$ for ZnO,[46] and eq 1, the carrier concentration N_D is calculated to be $(5.5 \pm 0.9) \times 10^{17}$ cm^{-3}, consistent with previously reported values for undoped ZnO.[47,48]

DISCUSSION

Morphology Study. Our AFM studies indicate that carboxylic acids, alcohols, and amines bind only very weakly on ZnO$(10\bar{1}0)$ surfaces. The poor binding of carboxylic acids is important because carboxylic acid groups are commonly used in applications such as dye-sensitized solar cells. We also observe the etching of ZnO by carboxylic acids, consistent with previous reports.[49]

In contrast, our data show that $C_{16}H_{33}PO_3H_2$ and $C_{18}H_{37}SH$ molecules bind to the surface and do not necessarily result in etching. The angle-dependent XPS measurements in Figure 6 show that $-PO_3H_2$ and −SH bind to ZnO with the alkyl chains oriented away from the surface. The C−H vibrational frequencies of both surface-bound molecules are consistent with closely packed alkyl chains, and the molecular coverage as measured by XPS is also in the range expected for dense layers. However, the AFM experiments show pronounced differences between the surface morphologies of the resulting thiol and phosphonic acid films.

Our data show that whereas the FTIR frequencies of the C−H vibrational modes suggest dense layers, phosphonic acid groups actually form islands rather than a continuous film. Our data show that surface functionalization with hexadecylphosphonic acid yields small nanoclusters that then grow into larger islands. Although these islands might connect with each other, they do not fuse into a homogeneous monolayer. Our AFM data suggest that the binding of the phosphonic acids to the surface is surprisingly weak, since we found that they can be removed from the surface using an AFM tip with very small applied forces (<40 nN). More than 1 μN is required to remove thiol molecules from ZnO surfaces. From previous AFM imaging studies, hexadecylphosphonic acids are known to form rough films on other surfaces, and whether they bind to substrates covalently is still controversial.[50−52] Our AFM scratching and XPS Zn $2p_{3/2}$ elemental scanning results suggest that they do not bind to the surface covalently but rather assemble through the hydrogen bonding of their head groups and the van der Waals interaction of their tails.[52]

Our AFM, FTIR, and XPS data all demonstrate that thiol groups provide uniform, dense, strongly bonded monolayers on the Zn$(10\bar{1}0)$ surface. However, the thiol etches ZnO surfaces at longer immersion times (less than 1 day), consistent with the results of frequency generation (SFG) experiments that reported the disorder of thiol layers at longer grafting times.[24]

Surface Photovoltage Measurements (SPV) and the Mott−Schottky Plots. Our SPV data indicate that the grafting of phosphonic acid and thiols reduces the band bending of the ZnO surface under ambient conditions. The surface photovoltage measurements show that upon illumination the amount of initial charge separation is smaller on ZnO samples grafted with either hexadecylphosphonic acid or octadecanethiol compared to that observed on the clean ZnO sample. Because the bulk optical properties (and therefore the number and depth distribution of electron−hole pairs created) are the same for each sample, we attribute the reduced charge separation on the functionalized samples to reduced band bending on the functionalized samples.

The reduced band bending is also supported by the decay parts of the curves in Figure 7a. Soon after the pulsed laser is off, the charges on the capacitors in the *RC* circuit recombine, and the band bending that drove the charge separation upon illumination now acts as a barrier to recombination. The average recombination times of the sample are ZnO-bare (4.9 μs) > ZnO-$C_{16}H_{33}PO_3H_2$ (2.2 μs) > ZnO-$C_{18}H_{37}SH$ (0.44 μs). Assuming that the sample with the largest band bending has the largest barrier to recombination,[35] the amount of band-bending is also ZnO-bare > ZnO-$C_{16}H_{33}PO_3H_2$ > ZnO-$C_{18}H_{37}SH$.

Our Mott−Schottky data show that the trends in band-bending inferred from SPV measurements are also valid at the ZnO−liquid interface. The linear parts of the Mott−Schottky plots reveal flat-band potentials of −0.20 V, 0.03 and 0.14 V versus $Ag/AgNO_3$ for ZnO-bare, ZnO-$C_{18}H_{37}SH$, and ZnO-$C_{16}H_{33}PO_3H_2$ respectively. The flat-band potential represents the electrochemical potential at which the bands have constant energy out to the surface. Bare ZnO has the most negative flat-band potential, so both modifications reduce the band-bending of ZnO. The nonlinear behaviors of the Mott−Schottky curves have been attributed to the surface states of the ZnO samples and will be discussed later.[34,35]

The width of the band-bending region, also called the space-charge region, can be estimated from the measured effective capacitance. For example, when ZnO has the same potential as the reference electrode ($\Psi_{ZnO} = 0$), the space-charge capacitance C_{ZnO} is estimated to be ∼0.11 μF for ZnO-bare, ∼0.13 μF for ZnO-$C_{18}H_{37}SH$, and ∼0.14 μF for ZnO-$C_{16}H_{33}PO_3H_2$ samples with an area of 3.8×10^{-5} m^2. The space-charge region width can be estimated by $w = \varepsilon\varepsilon_0 A/C_{ZnO}$[35] For area $A = (3.8 \pm 0.3) \times 10^{-5}$ m^2, vacuum permittivity $\varepsilon_0 = 8.85 \times 10^{-12}$ F/m, ZnO permittivity $\varepsilon = 8.5$,[46] the width of the space-charge region at a potential of 0 V (vs $Ag/AgNO_3$) is ∼26 ± 2 nm for ZnO-bare, ∼22 ± 2 nm for ZnO-$C_{18}H_{37}SH$, and ∼20 ± 2 nm for ZnO-$C_{16}H_{33}PO_3H_2$.

ZnO Surface Potential. Band-bending of ZnO at the space-charge layer comes from the partial ionization of ZnO surface groups.[35] Bare ZnO surfaces are often partially ionized from ZnOH to Zn−O^- termination and are negatively charged.[35] From the Mott−Schottky plots, we measured flat-band potentials at relatively negative potentials, −0.42 V versus $Ag/AgNO_3$, for bare ZnO. However, when the surfaces are passivated by the thiol molecules, the surface Zn−OH groups are replaced by Zn-$SC_{18}H_{37}$ bonds.[25] The density of the negative charge is reduced, and a flat-band potential near −0.21 V is observed. When the surfaces are covered by the phosphonic acid molecules, the surface Zn−OH groups are replaced by $ZnO_3HPC_{16}H_{33}$ groups and the ZnO surface is relatively neutral. As such, a flat-band

dx.doi.org/10.1021/la301347t | *Langmuir* 2012, 28, 10437−10445

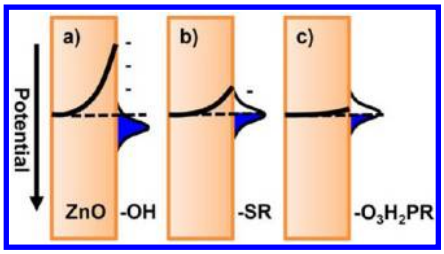

Figure 9. Schematic of the energy diagrams of (a) ZnO-bare, (b) ZnO-$C_{18}H_{37}SH$ and (c) ZnO-$C_{16}H_{33}PO_3H_2$. The peaks indicate the surface states (drawing not to scale).

potential of 0 V versus $Ag/AgNO_3$ is observed for the phosphonic acid-modified ZnO samples (Figure 9).

The nonlinear parts of the Mott–Schottky curves arise from the dynamic ionization of the surface molecules. For the Mott–Schottky relationship to hold, it is assumed that the surface charge does not change with the applied potential on the ZnO electrode.[35] This is a reasonable assumption when a positive potential is applied to the ZnO electrode. However, when negative potentials are applied to ZnO, the surface groups are ionized and the surface charge density changes. The negative potential injects electrons into the surface groups and makes the surface more negatively charged. These charges move the ZnO surface potential to more negative potentials. Because the capacitance of the ZnO space-charge layer is directly dependent on the surface potential as described in eq 1, the shifting surface potential results in the nonlinear behavior of the Mott–Schottky curves.

CONCLUSIONS

The ability of the octadecanoic acid, undecanol, dodecylamine, hexadecylphosphonic acid, and octadecanethiol to form a stable self-assembled monolayer on ZnO $(10\bar{1}0)$ surfaces is investigated. The octadecanoic acid, undecanol, and dodecylamine bind weakly on the ZnO $(10\bar{1}0)$ surface, and the hexadecylphosphonic acids and the octadecanethiol bind more strongly. When grafted under mild conditions, the octadecanoic acid, dodecylamine, and undecanol are easily rinsed away by solvents from the surface. Significant etching of the surfaces by the octadecanoic acid is observed. The hexadecylphosphonic acid and octadecanethiol survive rinsing, but their binding strengths and morphologies are very different. The hexadecylphosphonic acid forms small clusters and then larger islands on ZnO$(10\bar{1}0)$ surfaces. Octadecanethiol forms a uniform monolayer but etches the surface after longer immersion times. Octadecanethiols bind strongly on ZnO$(10\bar{1}0)$ surfaces with Zn–S bonds, and hexadecylphosphonic acids are probably held by hydrogen bonds. Surface photovoltage measurements and electrochemical impedance measurements of the ZnO samples reveal that the band-bending of ZnO$(10\bar{1}0)$ is reduced after phosphonic acid and thiol grafting. The flat-band potentials are ~−0.42 V for bare ZnO$(10\bar{1}0)$, ~−0.21 V for $C_{18}H_{37}SH$-modified ZnO$(10\bar{1}0)$, and ~0.0 V for $C_{16}H_{33}PO_3H_2$-modified ZnO$(10\bar{1}0)$ in 0.1 M TBAPF/acetonitrile versus $Ag/AgNO_3$ (0.01 M).

ASSOCIATED CONTENT

Supporting Information

AFM scratching data, detailed XPS data and calculations, and Mott–Schottky plots measured at different frequencies. This material is available free of charge via the Internet at http://pubs.acs.org.

AUTHOR INFORMATION

Corresponding Author

*E-mail: rjhamers@wisc.edu.

Notes

The authors declare no competing financial interest.

ACKNOWLEDGMENTS

This work was funded by the Division of Chemical Sciences, Geosciences, and Biosciences, Office of Basic Energy Sciences of the U.S. Department of Energy through grant no. DE-FG02-09ER16122.

REFERENCES

(1) Özgür, Ü.; Alivov, Y. I.; Liu, C.; Teke, A.; Reshchikov, M. A.; Doğan, S.; Avrutin, V.; Cho, S.-J.; Morkoç, H. A Comprehensive Review of ZnO Materials and Devices. *J. Appl. Phys.* **2005**, *98*, 041301–1–041301–103.

(2) Law, M.; Greene, L. E.; Johnson, J. C.; Saykally, R.; Yang, P. Nanowire Dye-Sensitized Solar Cells. *Nat. Mater.* **2005**, *4*, 455–459.

(3) Gonzalez-Valls, I.; Lira-Cantu, M. Vertically-Aligned Nanostructures of ZnO for Excitonic Solar Cells: A Review. *Energy Environ. Sci.* **2009**, *2*, 19–34.

(4) Pearton, S. *GaN and ZnO-Based Materials and Devices*; Springer: New York, 2012.

(5) Look, D. C.; Reynolds, D. C.; Sizelove, J. R.; Jones, R. L.; Litton, C. W.; Cantwell, G.; Harsch, W. C. Electrical Properties of Bulk ZnO. *Solid State Commun.* **1998**, *105*, 399–401.

(6) Galoppini, E.; Rochford, J.; Chen, H.; Saraf, G.; Lu, Y.; Hagfeldt, A.; Boschloo, G. Fast Electron Transport in Metal Organic Vapor Deposition Grown Dye-Sensitized ZnO Nanorod Solar Cells. *J. Phys. Chem. B* **2006**, *110*, 16159–16161.

(7) Lin, C.-Y.; Lai, Y.-H.; Chen, H.-W.; Chen, J.-G.; Kung, C.-W.; Vittal, R.; Ho, K.-C. Highly Efficient Dye-Sensitized Solar Cell with a ZnO Nanosheet-Based Photoanode. *Energy Environ. Sci.* **2011**, *4*, 3448–3455.

(8) Taratula, O.; Galoppini, E.; Mendelsohn, R.; Reyes, P. I.; Zhang, Z.; Duan, Z.; Zhong, J.; Lu, Y. Stepwise Functionalization of ZnO Nanotips with DNA. *Langmuir* **2009**, *25*, 2107–2113.

(9) Zhang, F.; Wang, X.; Ai, S.; Sun, Z.; Wan, Q.; Zhu, Z.; Xian, Y.; Jin, L.; Yamamoto, K. Immobilization of Uricase on ZnO Nanorods for a Reagentless Uric Acid Biosensor. *Anal. Chim. Acta* **2004**, *519*, 155–160.

(10) Corso, C. D.; Dickherber, A.; Hunt, W. D. An Investigation of Antibody Immobilization Methods Employing Organosilanes on Planar ZnO Surfaces for Biosensor Applications. *Biosens. Bioelectron.* **2008**, *24*, 805–811.

(11) Fu, Y. Q.; Luo, J. K.; Du, X. Y.; Flewitt, A. J.; Li, Y.; Markx, G. H.; Walton, A. J.; Milne, W. I. Recent Developments on ZnO Films for Acoustic Wave Based Bio-Sensing and Microfluidic Applications: A Review. *Sens. Actuators, B* **2010**, *143*, 606–619.

(12) Keis, K.; Magnusson, E.; Lindström, H.; Lindquist, S.-E.; Hagfeldt, A. A 5% Efficient Photoelectrochemical Solar Cell Based on Nanostructured ZnO Electrodes. *Sol. Energy Mater. Sol. Cells* **2002**, *73*, 51–58.

(13) Luo, B.; Rossini, J. E.; Gladfelter, W. L. Zinc Oxide Nanocrystals Stabilized by Alkylammonium Alkylcarbamates. *Langmuir* **2009**, *25*, 13133–13141.

(14) Tiwana, P.; Docampo, P.; Johnston, M. B.; Snaith, H. J.; Herz, L. M. Electron Mobility and Injection Dynamics in Mesoporous ZnO, SnO_2, and TiO_2 Films Used in Dye-Sensitized Solar Cells. *ACS Nano* **2011**, *5*, 5158–5166.

(15) Němec, H.; Rochford, J.; Taratula, O.; Galoppini, E.; Kužel, P.; Polívka, T.; Yartsev, A.; Sundström, V. Influence of the Electron-Cation Interaction on Electron Mobility in Dye-Sensitized ZnO and TiO_2 Nanocrystals: A Study Using Ultrafast Terahertz Spectroscopy. *Phys. Rev. Lett.* **2010**, *104*, 197401–1–197401–4.

(16) Taratula, O.; Galoppini, E.; Wang, D.; Chu, D.; Zhang, Z.; Chen, H. H.; Saraf, G.; Lu, Y. C. Binding Studies of Molecular Linkers to ZnO and MgZnO Nanotip Films. *J. Phys. Chem. B* **2006**, *110*, 6506−6515.
(17) Rochford, J.; Galoppini, E. Zinc(II) Tetraarylporphyrins Anchored to TiO_2, ZnO, and ZrO_2 Nanoparticle Films through Rigid-Rod Linkers. *Langmuir* **2008**, *24*, 5366−5374.
(18) Taratula, E.; Galoppini, E.; Mendelsohn, R. Stepwise Functionalization of ZnO Nanotips with DNA. *Langmuir* **2009**, *25*, 2107−2113.
(19) Moreira, N. H.; da Rosa, A. L.; Frauenheim, T. Covalent Functionalization of ZnO Surfaces: A Density Functional Tight Binding Study. *Appl. Phys. Lett.* **2009**, *94*, 193109−1−193109−3.
(20) Shi, X. Q.; Xu, H.; Van Hove, M. A.; Moreira, N. H.; Rosa, A. L.; Frauenheim, T. Substrate Mediated Stabilization of Methylphosphonic Acid on ZnO Non-polar Surfaces. *Surf. Sci.* **2012**, *606*, 289−292.
(21) Diebold, U.; Li, S. C.; Schmid, M. Oxide Surface Science. *Annu. Rev. Phys. Chem.* **2010**, *61*, 129−148.
(22) Batzill, M.; Diebold, U. Surface Studies of Gas Sensing Metal Oxides. *Phys. Chem. Chem. Phys.* **2007**, *9*, 2307−2318.
(23) Perkins, C. L. Molecular Anchors for Self-Assembled Monolayers on ZnO: A Direct Comparison of the Thiol and Phosphonic Acid Moieties. *J. Phys. Chem. C* **2009**, *113*, 18276−18286.
(24) Hedberg, J.; Leygraf, C.; Cimatu, K.; Baldelli, S. Adsorption and Structure of Octadecanethiol on Zinc Surfaces as Probed by Sum Frequency Generation Spectroscopy, Imaging, and Electrochemical Techniques. *J. Phys. Chem. C* **2007**, *111*, 17587−17596.
(25) Sadik, P. W.; Pearton, S. J.; Norton, D. P. Functionalizing Zn- and O-Terminated ZnO with Thiols. *J. Appl. Phys.* **2007**, *101*, 104514−1−104514−5.
(26) Liu, D.; Wu, W.; Qiu, Y.; Yang, S.; Xiao, S.; Wang, Q.-Q.; Ding, L.; Wang, J. Surface Functionalization of ZnO Nanotetrapods with Photoactive and Electroactive Organic Monolayers. *Langmuir* **2008**, *24*, 5052−5059.
(27) Hotchkiss, P. J.; Malicki, M.; Giordano, A. J.; Armstrong, N. R.; Marder, S. R. Characterization of Phosphonic Acid Binding to Zinc Oxide. *J. Mater. Chem* **2011**, *21*, 3107−3112.
(28) Ruther, R. E.; Franking, R.; Huhn, A. M.; Gomez-Zayas, J.; Hamers, R. J. Formation of Smooth, Conformal Molecular Layers on ZnO Surfaces via Photochemical Grafting. *Langmuir* **2011**, *27*, 10604−10614.
(29) Kobayashi, A.; Ohta, J.; Fujioka, H. Characteristics of Single Crystal ZnO Annealed in a Ceramic ZnO Box and Its Application for Epitaxial Growth. *Jpn. J. Appl. Phys.* **2006**, *45*, 5724−5727.
(30) Moulder, J. F.; Stickle, W. F.; Sobol, P. E.; Bomben, K. D. *Handbook of X-ray Photoelectron Spectroscopy*; Perkin-Elmer: Eden Prairie, MN, 1992.
(31) Wojdyr, M. Fityk (free software), version 0.9.3, 2009.
(32) Chen, J.; Franking, R.; Ruther, R. E.; Tan, Y.; He, X.; Hogendoorn, S. R.; Hamers, R. J. Formation of Molecular Monolayers on TiO_2 Surfaces: A Surface Analogue of the Williamson Ether Synthesis. *Langmuir* **2011**, *27*, 6879−6889.
(33) Scholz, F. In *Electroanalytical Methods: Guide to Experiments and Applications*; Springer-Verlag: Heidelberg, 2002; p 298.
(34) Parthasarathy, M.; Ramgir, N. S.; Sathe, B. R.; Mulla, I. S.; Pillai, V. K. Surface-State-Mediated Electron Transfer at Nanostructured ZnO Multipod/Electrolyte Interfaces. *J. Phys. Chem. C* **2007**, *111*, 13092−13102.
(35) Gomes, W. P.; Cardon, F. Electron Energy Levels in Semiconductor Electrochemistry. *Prog. Surf. Sci.* **1982**, *12*, 155−216.
(36) Carpick, R. W.; Salmeron, M. Scratching the Surface: Fundamental Investigations of Tribology with Atomic Force Microscopy. *Chem. Rev.* **1997**, *97*, 1163−1194.
(37) Porter, M. D.; Bright, T. B.; Allara, D. L.; Chidsey, C. E. D. Spontaneously Organized Molecular Assemblies. 4. Structural Characterization of *n*-Alkyl Thiol Monolayers on Gold by Optical Ellipsometry, Infrared Spectroscopy, and Electrochemistry. *J. Am. Chem. Soc.* **1987**, *109*, 3559−3568.
(38) Nuzzo, R. G.; Zegarski, B. R.; Dubois, L. H. Fundamental Studies of the Chemisorption of Organosulfur Compounds on Au(111). Implications for Molecular Self-Assembly on Gold Surfaces. *J. Am. Chem. Soc.* **1987**, *109*, 733−740.
(39) Rodriguez, J. A.; Jirsak, T.; Chaturvedi, S.; Kuhn, M. Reaction of SO_2 with ZnO(000-1)-O and ZnO Powders: Photoemission and XANES Studies on the Formation of SO_3 and SO_4. *Surf. Sci.* **1999**, *442*, 400−412.
(40) Castner, D. G.; Hinds, K.; Grainger, D. W. X-Ray Photoelectron Spectroscopy Sulfur 2p Study of Organic Thiol and Disulfide Binding Interactions with Gold Surfaces. *Langmuir* **1996**, *12*, 5083−5086.
(41) Tan, Z.; Xia, Y.; Zhao, M.; Liu, X.; Li, F.; Huang, B.; Ji, Y. Electron Stopping Power and Mean Free Path in Organic Compounds over the Energy Range of 20−10,000 eV. *Nucl. Instrum. Methods Phys. Res., Sect. B* **2004**, *222*, 27−43.
(42) Smith, C. C. Evaluation of a Simple Correction for the Hydrocarbon Contamination Layer in Quantitative Surface Analysis by XPS. *J. Electron Spectrosc.* **2005**, *148*, 21−28.
(43) Cumpson, P. J. Angle-Resolved XPS and AES: Depth-Resolution Limits and a General Comparison of Properties of Depth-Profile Reconstruction Methods. *J. Electron Spectrosc.* **1995**, *73*, 25−52.
(44) Hamann, T. W.; Gstrein, F.; Brunschwig, B. S.; Lewis, N. S. Measurement of the Dependence of Interfacial Charge-Transfer Rate Constants on the Reorganization Energy of Redox Species at n-ZnO/H_2O Interfaces. *J. Am. Chem. Soc.* **2005**, *127*, 13949−13954.
(45) Sukhotin, A. M.; Grilikhes, M. S.; Lisovaya, E. V. The Influence of Passivation on the Kinetics of the Dissolution of Iron—I. Outer Layer of the Passivating Film as a Heavy Doped Thin Semiconductor and Mott-Shottky Equation. *Electrochim. Acta* **1989**, *34*, 109−112.
(46) Morrison, S. R. *Electrochemistry at Semiconductor and Oxidized Metal Electrodes*; Plenum Press: New York, 1980.
(47) Windisch, C. F., Jr.; Exarhos, G. J. Mott-Schottky Analysis of Thin ZnO Films. *J. Vac. Sci. Technol., A* **2000**, *18*, 1677−1680.
(48) Gelderman, K.; Lee, L.; Donne, S. W. Flat-Band Potential of a Semiconductor: Using the Mott-Schottky Equation. *J. Chem. Educ.* **2007**, *84*, 685−688.
(49) González-Moreno, R.; Cook, P. L.; Zegkinoglou, I.; Liu, X.; Johnson, P. S.; Yang, W.; Ruther, R. E.; Hamers, R. J.; Tena-Zaera, R.; Himpsel, F. J.; Ortega, J. E.; Rogero, C. Attachment of Protoporphyrin Dyes to Nanostructured ZnO Surfaces: Characterization by Near Edge X-ray Absorption Fine Structure Spectroscopy. *J. Phys. Chem. C* **2011**, *115*, 18195−18201.
(50) Valtiner, M.; Borodin, S.; Grundmeier, G. Stabilization and Acidic Dissolution Mechanism of Single-Crystalline ZnO(0001) Surface in Electrolytes Studied by in-Situ AFM Imaging and ex-Situ LEED. *Langmuir* **2008**, *24*, 5350−5358.
(51) Zhang, B.; Kong, T.; Xu, W.; Su, R.; Gao, Y.; Cheng, G. Surface Functionalization of Zinc Oxide by Carboxyalkylphosphonic Acid Self-Assembled Monolayers. *Langmuir* **2010**, *26*, 4514−4522.
(52) Gawalt, E. S.; Avaltroni, M. J.; Koch, N.; Schwartz, J. Self-Assembly and Bonding of Alkanephosphonic Acids on the Native Oxide Surface of Titanium. *Langmuir* **2001**, *17*, 5736−5738.